
Multimodal Learning for Arcing Detection in Pantograph-Catenary Systems

Hao Dong^{1,2} Eleni Chatzi¹ Olga Fink²

¹Chair of Structural Mechanics & Monitoring, ETH Zürich

²Intelligent Maintenance and Operations Systems Lab, EPFL

Abstract

The pantograph-catenary interface is essential for ensuring uninterrupted and reliable power delivery in electrified rail systems. However, electrical arcing at this interface poses serious risks, including accelerated wear of contact components, degraded system performance, and potential service disruptions. Detecting arcing events at the pantograph-catenary interface is challenging due to their transient nature, noisy operating environment, data scarcity, and the difficulty of distinguishing arcs from other similar transient phenomena. To address these challenges, we propose a novel multimodal framework that combines high-resolution image data with force measurements to more accurately and robustly detect arcing events. First, we construct two arcing detection datasets comprising synchronized visual and force measurements. One dataset is built from data provided by the Swiss Federal Railways (SBB), and the other is derived from publicly available videos of arcing events in different railway systems and synthetic force data that mimic the characteristics observed in the real dataset. Leveraging these datasets, we propose MultiDeepSAD, an extension of the DeepSAD algorithm for multiple modalities with a new loss formulation. Additionally, we introduce tailored pseudo-anomaly generation techniques specific to each data type, such as synthetic arc-like artifacts in images and simulated force irregularities, to augment training data and improve the discriminative ability of the model. Through extensive experiments and ablation studies, we demonstrate that our framework significantly outperforms baseline approaches, exhibiting enhanced sensitivity to real arcing events even under domain shifts and limited availability of real arcing observations. To the best of our knowledge, this is the first method and publicly available dataset that integrates image and force data for pantograph-catenary arcing event detection. The proposed framework offers a practical solution for real-time monitoring of arcing events in pantograph-catenary systems, ultimately contributing to safer and more reliable railway operations. Our source code and dataset will be available at <https://github.com/EPFL-IMOS/Multimodal-Arcing>.

1 Introduction

The pantograph-catenary system serves as the critical interface for power transmission to electric trains, ensuring continuous and reliable operation across electrified rail networks [10, 9, 43, 58]. Reliable electrical contact at this interface is essential for the safe and efficient functioning of railway systems, supplying uninterrupted power for both traction and onboard services [7, 62, 19, 57, 18]. Any disruption at this interface can lead to operational delays, diminished performance, and potential damage to the complex electrical equipment involved. The growing global demand for efficient, reliable and modern rail transport, spanning both passenger and freight services, highlights the need for dependable power delivery, thereby increasing the importance of detecting and mitigating

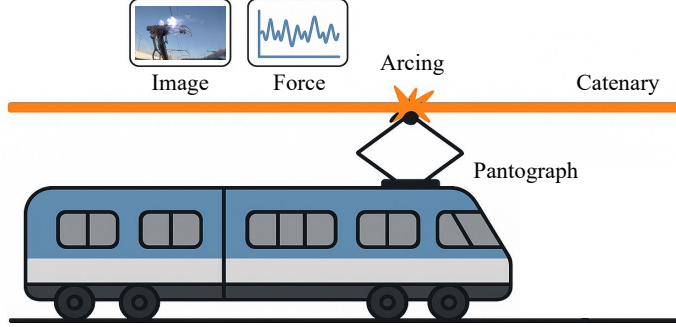


Figure 1: Proposed solution for arcing detection in pantograph-catenary systems with image and force measurements.

anomalies such as electrical arcing in the pantograph-catenary system [2, 8]. As operational demands on rail systems intensify, whether due to increased speed, higher frequency of service, or heavier loads, the dynamic interaction between the pantograph and the catenary becomes more complex, increasing the risk of contact loss and subsequent arcing. Therefore, effective arcing detection and assessment of their contribution to degradation is increasingly important for maintaining reliable operation across different service conditions [20, 41].

Electrical arcing in pantograph-catenary systems is a sporadic phenomenon that stems from insufficient contact between the pantograph contact strip and the overhead catenary wire [32]. Poor contact conditions can be attributed to a number of factors, including inherent vibrations of the pantograph, irregularities in the geometry of the contact line, the presence of hard spots on the contact surfaces, and the passage of the train over electrical neutral zones [20]. Furthermore, environmental effects, such as the formation of ice on contact surfaces during colder periods, can also contribute to the initiation of arcing. The generation of an electric arc is accompanied by the production of intense heat, which, over time, leads to the degradation and erosion of both the sliding plate of the pantograph and the catenary wire itself [59]. Without continuous monitoring and timely mitigation, repeated arcing events can accumulate damage to both the pantograph and the catenary infrastructure, requiring costly maintenance interventions and potentially resulting in significant disruptions to railway services [32]. Beyond direct physical damage, arcing events also generate electromagnetic disturbances that can pose a threat to the electromagnetic compatibility and safety of the trains and may interfere with vital communication systems utilized for railway signaling and control. The high temperatures generated by arcing accelerate contact-surface wear, progressively degrading contact quality and increasing the likelihood of further arcing without sustained monitoring and maintenance. Arcing is, thus, not merely a sign of poor contact, but a destructive process that actively accelerates deterioration, highlighting the importance of continuous monitoring and assessment of cumulative arcing activity to minimize its long-term impact on railway infrastructure and operational reliability.

Traditional methods for detecting arcing in pantograph-catenary systems have primarily relied on analyzing electrical signals, such as voltage and current, within the power supply system [4, 30, 65]. However, arcing-induced signatures can often be masked by noise and other electrical phenomena in these signals, making detection a challenging task that requires advanced feature extraction and algorithm design [35]. In response to the limitations of traditional electrical signal-based methods, growing interest has turned to leveraging image processing and computer vision techniques for arcing detection [64]. These methods provide a non-contact means of monitoring the pantograph-catenary interface, enabling the identification of the distinctive visual signatures associated with electrical arcing. Complementary to visual methods, force and accelerometer data offer valuable insights into the mechanical interaction between the pantograph and the catenary [55]. Such sensors can detect events such as contact loss or excessive vibration, which often precede or accompany the occurrence of electrical arcs.

In this research, we propose a unified, multimodal framework that integrates image and contact force measurements to achieve more robust and accurate arcing detection (Fig. 1). By leveraging the complementary information of both visual and mechanical sensing, our approach offers a reliable solution for monitoring pantograph-catenary system health, particularly under complex operational conditions. Due to the absence of public datasets for railway arcing detection, we first create two

arching detection datasets comprising synchronized visual and force measurements. One dataset is derived from data provided by Swiss Federal Railways (SBB), while the other is collected from publicly available internet videos and synthetic force data. The second dataset will be publicly released to facilitate future research in this domain. We then propose MultiDeepSAD, an extension of DeepSAD [51] adapted to multimodal settings with *a new loss formulation*, and develop modality-specific *pseudo-anomaly generation strategies* for both image and force inputs. These pseudo-anomalies are then used to train MultiDeepSAD, enabling improved arcing detection performance. Extensive experiments and ablation studies demonstrate the robustness of our framework across varying numbers of real anomaly samples for pseudo-anomaly generation and domain shifts. Our contributions can be summarized as follows:

- We propose MultiDeepSAD, a universal framework for multimodal arcing detection in pantograph-catenary systems, incorporating both a new training objective and modality-specific pseudo-anomaly generation strategies.
- We release a new multimodal dataset that includes synchronized visual and force measurements, which can serve as a challenging benchmark for future research on arcing detection in pantograph-catenary systems.
- Extensive experiments and ablation studies across both datasets consistently demonstrate the effectiveness and robustness of the proposed framework.

2 Related Work

Current/Voltage-based Arcing Detection. Early arcing detection methods primarily relied on handcrafted features [42], including basic time-domain statistical analysis and frequency-domain methods like the Fast Fourier Transform [15]. To better analyze the non-stationary nature of arc transients, more advanced time-frequency techniques such as the Wavelet Transform and the Hilbert-Huang Transform [5] were introduced, enabling simultaneous localization of arc events in both time and frequency. The field has increasingly transitioned towards machine learning-based methods, first employing models like Support Vector Machines [4] that rely on handcrafted features extracted from these signals. Besides, other methods that combine the Discrete Wavelet Transform with deep neural networks have become prominent [66]. This approach leverages the Wavelet transform to decompose the signal, allowing the neural network to automatically learn complex fault characteristics from the resulting time-frequency data, achieving high recognition accuracy.

Image-based Arcing Detection. Instead of relying on current or voltage measurements—which are often unavailable, noisy, and highly dependent on sensor placement and operating conditions—recent research has increasingly focused on visual inputs, as arcing typically manifests as distinctive light emission and sparks that can be captured by onboard cameras and processed robustly with modern vision models [30, 40, 22, 37]. High-speed cameras were used to capture the transient nature of arcing, with subsequent image processing techniques developed to isolate and characterize arc events [2]. More recent advances have leveraged machine learning algorithms to automate the detection and classification of arcing events, thereby improving both accuracy and robustness [31, 47, 41]. For example, Quan et al [48] introduce a dual-branch semantic segmentation model designed for robust pantograph-catenary arcing detection. The architecture features a Semantic Feature Branch that captures multi-scale global context and a parallel Detail Feature Branch that preserves high-resolution information to accurately segment small arcing events. A novel Feature Enhancement Mechanism subsequently fuses the outputs and employs a learnable visual center module to increase the feature discriminability between arcing and complex backgrounds, thereby improving model robustness. Building on the idea of multiscale representation, Liu et al. [41] utilize a Swin Transformer encoder to capture global context and a custom down-top multi-scale CNN decoder that fuses features from different levels to handle various arcing sizes. A key contribution is the Arc Feature Augmentation module, which leverages the inherent high luminosity of arcing by combining global max and threshold features to selectively amplify the arcing pixel representation, significantly improving detection in complex scenes. In a complementary direction, Yan et al. [64] address the challenge of detecting arcs with varying sizes and shapes by integrating a guided anchor mechanism that dynamically adjusts anchor generation based on arc characteristics, improving both efficiency and localization accuracy.

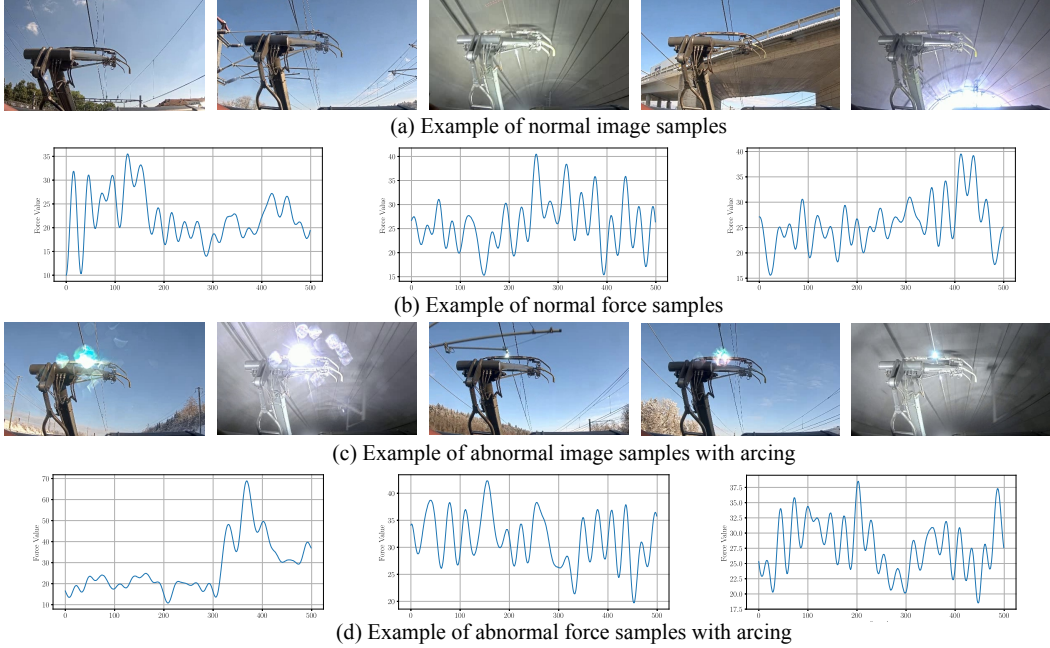


Figure 2: Representative samples from the SBB-AD dataset, consisting of time-synchronized pantograph camera images and corresponding contact-force measurements provided by SBB.

Force/Accelerometer-based Arcing Detection. Complementary to image-based methods, sensor data from force sensors and accelerometers have been used to capture the mechanical vibrations and dynamic loads associated with arcing [61, 17, 24]. Such approaches take advantage of the fact that electrical arcing can produce detectable force disturbances and vibrational signatures in the pantograph-catenary system [28]. Researchers have developed signal processing pipelines to extract characteristic patterns from these sensors, which can be correlated with arc events [46, 21]. For example, in the preprocessing pipeline of Gregori et al. [24], raw acceleration signals are resampled to a common spatial domain to achieve speed-invariance, segmented into samples, and then standardized before being used as input for the networks.

Multimodal Arcing Detection. The integration of image data with other modalities is an emerging trend that addresses the limitations of single-modality approaches. By integrating information from visual and complementary sensors such as infrared and audio, it has become possible to mitigate false positives caused by environmental noise and sensor-specific artifacts. For example, Huang et al. [29] fuse RGB and infrared images using a convolutional neural network (CNN) for arc detection in visible-light images, a threshold method for infrared images, and a CNN-based environment perception model to dynamically adjust weights for each modality before fusing the results using evidence theory. Yan et al [63] propose a multimodal arc detection network that pretrains a Denoising Diffusion Probabilistic Model [27] on unlabeled infrared and visible light images for feature extraction and then fine-tunes a decoder that uses audio signals as semantic prompts to improve visual arc detection with limited data. Despite advancements in the field, the fusion of image and force data has been largely overlooked for arcing detection.

Pseudo-anomaly Generation. Since pantograph arcing events are rare, safety-critical, and often weakly labeled in real operational data, several recent works motivate framing arc detection as an anomaly detection problem, where pseudo-anomaly generation can provide additional supervision. Prior work on pseudo-anomaly generation has demonstrated that synthesizing realistic yet controllably abnormal samples can substantially enhance the training of anomaly detectors by providing a richer supervisory signal in the absence of labeled anomalies [13, 39, 44]. Early approaches leveraged simple perturbations, such as geometric transformations [23] or patch-level modifications [36], to create anomaly examples for one-class classifiers, while more recent methods employ deep generative models to produce high-fidelity anomalies that better mimic the complexity of real deviations [54, 52]. Furthermore, recent studies have explored semi-supervised paradigms, in which a small set of labeled anomalies guides the generation process [11], as well as adaptive techniques that dynamically

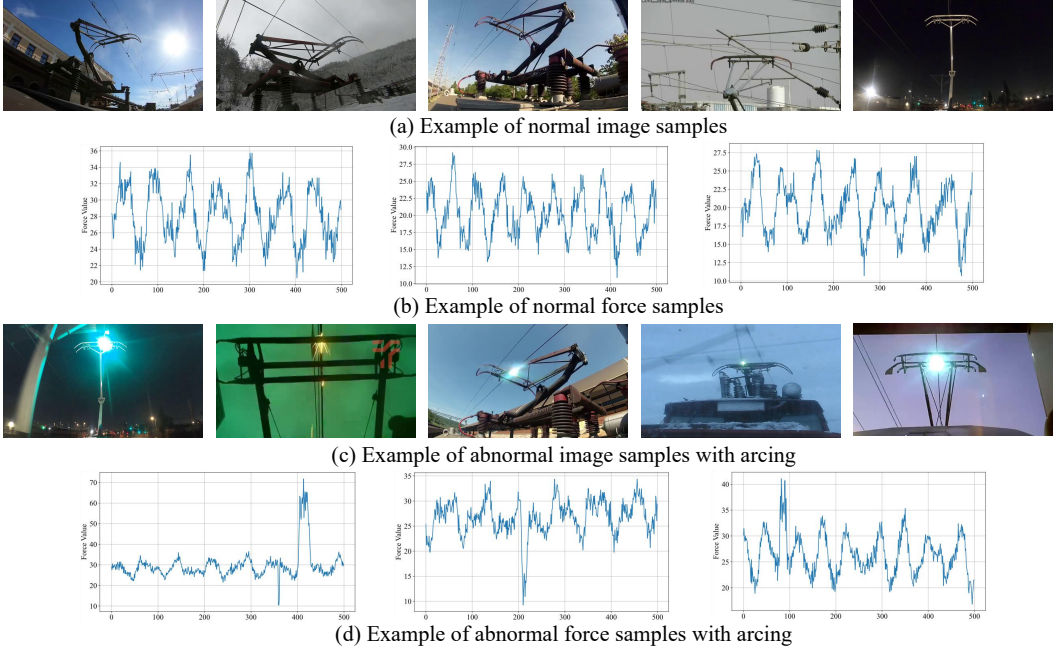


Figure 3: Examples from the Open-AD dataset, constructed from internet and simulation data.

adjust the difficulty of generated anomalies throughout training [34]. However, the intersection of multimodal learning and arcing event detection remains largely unexplored in current literature.

3 The Creation of Multimodal Arcing Detection Dataset

Due to the limited availability of public datasets for railway arcing detection, we construct two arcing detection datasets to support our experiments.

3.1 Multimodal Arcing Detection Dataset from SBB Data

The first dataset, termed the SBB Arcing Detection Dataset (SBB-AD), is created using the data provided by our industrial partner SBB. This dataset includes synchronized image and force sensor data (Fig. 2), captured from an SBB diagnostic train operating in Switzerland. The data acquisition setup involved a camera focused on the pantograph-catenary system and a co-located force sensor measuring their contact force. The image data is recorded at 60 Hz, while the force data is sampled at 500 Hz. Collection campaigns were conducted in summer (August 8, 2022) and winter (January 19, 2023) to capture diverse acquisition conditions and background settings, including instances of tunnel passage, covering over 200 km in total. The dataset consists of 3,107 normal samples for training and a balanced test set of 328 samples, comprising 164 normal, 164 arcing anomaly instances. To generate these samples, recorded videos were segmented into one-second intervals, with all arcing events carefully identified and labeled. For each segment containing an arcing event, a representative frame capturing the arc and its corresponding one-second force data were selected. For segments without arcing, one frame was randomly sampled along with its corresponding force data to represent normal operation. Due to copyright restrictions imposed by SBB, this dataset is private and used solely for experimental purposes. To facilitate future research in this domain and benefit the community, we additionally construct a second dataset that is fully open-sourced.

3.2 Multimodal Arcing Detection Dataset from Internet and Simulation Data

The second dataset, termed the Open Arcing Detection Dataset (Open-AD), is constructed by combining internet-sourced video data with synthetic force data (Fig. 3). For the visual modality, we collect YouTube videos of pantograph-catenary systems that cover both normal operation and arcing events. For the force modality, we generate synthetic force signals under normal and abnormal conditions

using hand-crafted signal properties designed to approximate real-world operating characteristics. We then extract image frames from the videos and associate each frame with a simulated force signal: normal force signals are paired with normal images, whereas abnormal force signals are paired with images that contain arcing events.

3.2.1 Internet-sourced Data for Image Measurements

For the image measurements, we collect videos of pantograph-catenary systems from YouTube, covering both normal operation and arcing events. In total, we curate 23 videos spanning diverse weather and lighting conditions (e.g., sunny and snowy; daytime and nighttime), multiple pantograph-catenary configurations, and recordings from different countries, as shown in Fig. 3 (a) and (c). We extract all frames from the videos and manually annotate those containing arcing events. Overall, the resulting dataset contains 3,800 normal samples for training and a balanced test set of 484 samples, comprising 238 normal samples and 246 arcing anomaly instances.

3.2.2 Synthetic Data Generation for Force Measurements

Because the internet videos do not provide corresponding force measurements, we generate synthetic force signals that mimic pantograph-catenary interactions under both normal and abnormal conditions. Each measurement consists of 500 samples over a 1-second interval, corresponding to a sampling rate of 500 Hz, as shown in Fig. 3 (b) and (d).

Normal condition samples incorporate multiple sources of variability following the mathematical formulation:

$$F_{\text{normal}}(t) = F_{\text{mean}} + \sum_{i=1}^3 A_i \cdot \sin(2\pi f_i t + \phi_i) + \eta_{\text{meas}}(t) + \eta_{\text{irreg}}(t) + D(t) + T(t) + V(t), \quad (1)$$

where $F_{\text{mean}} \sim \mathcal{U}(20, 30)$ N is the randomized mean contact force; the oscillatory components have frequencies $f_1 \sim \mathcal{U}(6, 10)$ Hz, $f_2 \sim \mathcal{U}(10, 14)$ Hz, $f_3 \sim \mathcal{U}(18, 25)$ Hz with corresponding amplitudes $A_1 \sim \mathcal{U}(2.5, 4.5)$ N, $A_2 \sim \mathcal{U}(1.2, 2.5)$ N, $A_3 \sim \mathcal{U}(0.6, 1.6)$ N, and random phase offsets $\phi_i \sim \mathcal{U}(0, 2\pi)$; $\eta_{\text{meas}} \sim \mathcal{N}(0, 1.0)$ N and $\eta_{\text{irreg}} \sim \mathcal{N}(0, 0.6)$ N represent Gaussian measurement noise and wire irregularities; $D(t) = d \cdot t$ with $d \sim \mathcal{U}(-1.5, 1.5)$ N represents linear temporal drift; $T(t)$ represents transient disturbances (30% probability, Gaussian-shaped, ± 3 N amplitude, 10 – 40 ms duration); and $V(t)$ represents brief subtle arcing signatures. The mathematical formulation models the physical reality of pantograph-catenary contact force as a superposition of *deterministic mechanical oscillations and stochastic disturbances*. These normal variations are constructed to create ambiguity with abnormal events, ensuring classification requires detailed signal analysis rather than simple thresholds.

Abnormal condition samples contain three types of arcing events with varying severity: (1) *loss of contact arcing* (35% probability) causing 30 – 90% force drops with electrical noise and contact impulses; (2) *excessive contact force arcing* (30% probability) producing 40 – 150% force increases with mechanical vibrations and oscillatory decay; and (3) *subtle micro-arching* (35% probability) with minimal force perturbation (± 5 – 20%) but elevated high-frequency noise ($\sigma = 0.8$ N). Each abnormal sample contains 1 – 3 randomly positioned arcing events (5 – 30 samples duration), except 20% of abnormal samples that contain no discrete arcing events but only altered burst noise patterns ($\sigma = 1.2$ N over 20 – 60 ms regions), representing incipient fault conditions. This multi-level severity design with substantial intra-class variance ensures that successful detection requires sophisticated feature extraction beyond magnitude-based approaches.

4 Methodology

4.1 Problem Definition

Multimodal anomaly detection refers to the task of identifying data instances that exhibit significant deviations from the expected patterns within datasets comprising multiple heterogeneous modalities (e.g., image, force, etc.). These modalities may capture complementary aspects of a system or process, and their integration is crucial for robust anomaly identification. Formally, given a set of aligned

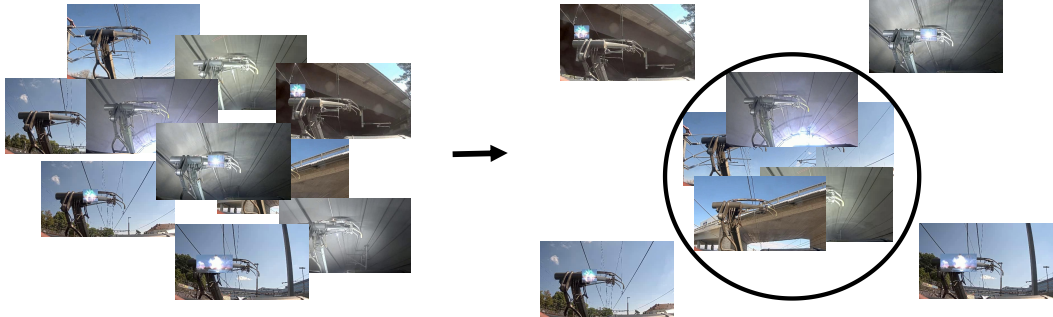


Figure 4: Illustration of the DeepSAD objective: normal samples are embedded close to a hypersphere center, while anomalous samples are pushed outside the hypersphere beyond a margin.

multimodal inputs:

$$\{(x^{(1)}, x^{(2)}, \dots, x^{(M)})\},$$

where each $x^{(m)} \in \mathcal{X}^{(m)}$ corresponds to the m -th modality and M is the total number of modalities, the objective is to learn a model:

$$f : \mathcal{X}^{(1)} \times \dots \times \mathcal{X}^{(M)} \rightarrow \{0, 1\},$$

that predicts whether a given multimodal instance is normal (0) or anomalous (1). A subset of the labels for $x^{(m)}$ can also be provided during training. The challenge lies in effectively modeling the complex intra- and inter-modal correlations to detect anomalies that may manifest in one or more modalities, while preserving robustness to noise or missing modalities.

4.2 Preliminaries

Deep Semi-Supervised Anomaly Detection (DeepSAD) [51] is a deep learning method designed to effectively identify anomalies by leveraging both normal data and a small set of labeled anomalies. It operates by training a neural network parameterized by weights \mathbf{W} to learn a mapping function $\phi(\cdot; \mathbf{W})$ from the input space $\mathcal{X} \subseteq \mathbb{R}^d$ to a lower-dimensional feature space $\mathcal{F} \subseteq \mathbb{R}^p$, such that $\mathbf{F} = \phi(x; \mathbf{W})$. The core objective of this transformation is twofold: to map normal data points to be tightly clustered around a pre-defined or learned center $\mathbf{c} \in \mathcal{F}$ within a hypersphere, and simultaneously to ensure that known anomalous data points are mapped outside this hypersphere. This is typically achieved by minimizing an objective function that incorporates these goals. For a set of normal samples \mathcal{D}_n and a set of labeled anomalous samples \mathcal{D}_a , the objective function can be generally formulated as:

$$\min_{\mathbf{W}} \frac{1}{|\mathcal{D}_n|} \sum_{x_i \in \mathcal{D}_n} \|\phi(x_i; \mathbf{W}) - \mathbf{c}\|^2 + \eta \frac{1}{|\mathcal{D}_a|} \sum_{x_j \in \mathcal{D}_a} (\|\phi(x_j; \mathbf{W}) - \mathbf{c}\|^2)^{-1}, \quad (2)$$

where $|\mathcal{D}_n|$ and $|\mathcal{D}_a|$ denote the number of elements in \mathcal{D}_n and \mathcal{D}_a . Here, the first term minimizes the squared Euclidean distance for normal samples to the center \mathbf{c} . The second term, weighted by $\eta > 0$, penalizes labeled anomalies $x_j \in \mathcal{D}_a$ and effectively pushes them away from the normal data cluster. If no labeled anomalies are available ($|\mathcal{D}_a| = 0$), the objective reduces to that of DeepSVDD [50], which focuses solely on compacting the normal data. In this case, the objective can be written as:

$$\min_{\mathbf{W}} \frac{1}{|\mathcal{D}_n|} \sum_{x_i \in \mathcal{D}_n} \|\phi(x_i; \mathbf{W}) - \mathbf{c}\|^2. \quad (3)$$

During inference, the anomaly score $s(x)$ for a new, unseen sample x is calculated as its squared Euclidean distance to the center \mathbf{c} in the learned feature space:

$$s(x) = \|\phi(x; \mathbf{W}^*) - \mathbf{c}\|^2, \quad (4)$$

where \mathbf{W}^* represents the optimized network weights. A sample x is classified as an anomaly if its score $s(x)$ exceeds a predefined threshold, which is often determined based on the distribution of scores on the training data (e.g., the 95th percentile). A higher score $s(x)$ indicates a greater deviation from the learned normality and thus a higher probability that the sample is an anomaly.

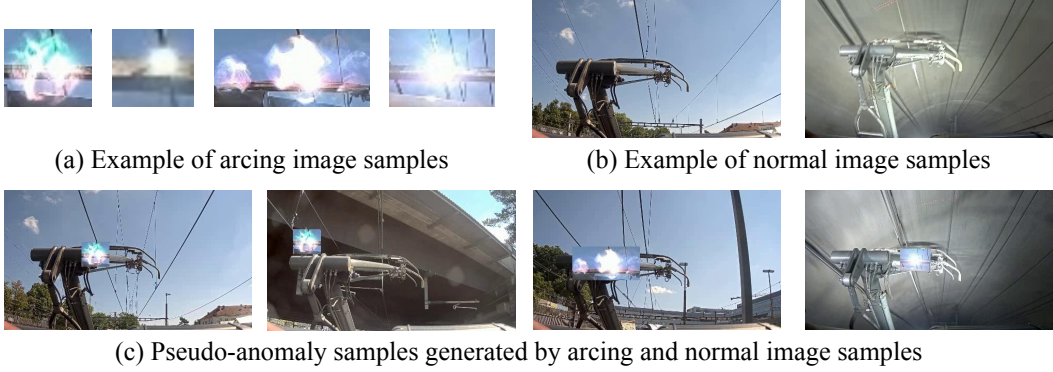


Figure 5: Illustration of pseudo-anomaly image samples generation, where we randomly paste arcing images onto pantographs in normal images.

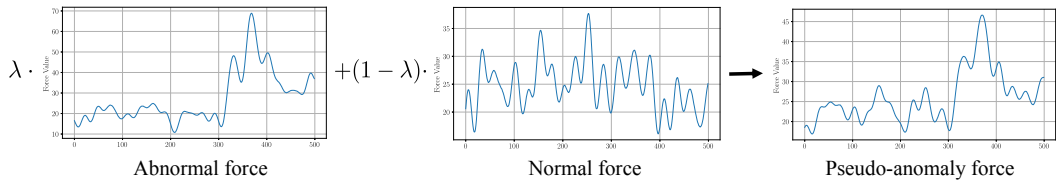


Figure 6: Illustration on pseudo-anomaly force sample generation, where we randomly combine samples from normal and abnormal force patterns. $\lambda \sim \text{Beta}(\alpha, \alpha)$ is a random value between 0 and 1.

4.3 Multimodal DeepSAD with Pseudo-anomaly Generation

In this work, we extend DeepSAD to the multimodal setting and develop effective pseudo-anomaly generation strategies for both image and force modalities. These pseudo-anomalies are then leveraged during training to improve the model’s arcing detection performance.

Pseudo-anomaly Image Sample Generation. Arcing events are rare and challenging to capture in real-world scenarios. As a result, supervised deep learning models often struggle to learn robust representations only a limited number of labeled anomalies are available. To address this challenge, we propose a pseudo-anomaly generation strategy that leverages a small set of labeled anomalies along together a large set of normal data. We first manually crop the arcing regions in the labeled anomaly samples (Fig. 5 (a)). Then, we generate synthetic anomalous image samples by randomly pasting the labeled arcing regions onto pantographs in normal images (Fig. 5 (b)), resulting in pseudo-anomalies with simulated arcing (Fig. 5 (c)). This approach allows us to generate an unlimited number of anomalous image samples, which are added to the anomaly set \mathcal{D}_a to improve training efficacy.

Pseudo-anomaly Force Sample Generation. Similarly, for the force modality, we assume access to a small set of real anomalous force signals along with a substantial amount of normal samples. Inspired by Mixup [68], we generate synthetic anomalous force signals by taking convex combinations of randomly selected abnormal and normal signals (Fig. 6):

$$\mathbf{d} = \lambda \mathbf{a}_1 + (1 - \lambda) \mathbf{a}_2, \quad (5)$$

where \mathbf{a}_1 and \mathbf{a}_2 represent abnormal and normal force samples, respectively, and $\lambda \sim \text{Beta}(\alpha, \alpha)$, for $\alpha \in (0, \infty)$. This method similarly enables the creation of an arbitrary number of pseudo-anomalous force samples, which are incorporated into \mathcal{D}_a .

Multimodal DeepSAD (MultiDeepSAD). The original DeepSAD framework is designed for unimodal inputs. We extend it to a multimodal setting by introducing dedicated mapping functions for each modality. Specifically, we define the encoder for each modality as follows: $\phi(\cdot; \mathbf{W}) = [\phi_1(\cdot; \mathbf{W}_1); \phi_2(\cdot; \mathbf{W}_2)]$, where $\phi_1(\cdot; \mathbf{W}_1)$ and $\phi_2(\cdot; \mathbf{W}_2)$ are modality-specific encoders for image and force inputs $x^{(1)}$ and $x^{(2)}$, respectively. The final multimodal representation $\mathbf{F} = \phi(x; \mathbf{W}) = \text{MLP}[\mathbf{F}_1; \mathbf{F}_2]$ is the concatenation of features $\mathbf{F}_1 = \phi(x_1; \mathbf{W}_1)$ and $\mathbf{F}_2 = \phi(x_2; \mathbf{W}_2)$ from both modalities followed by a multilayer perceptron. The inclusion of

Method	Force	Image	SBB-AD	Open-AD
IForest [38]	✓		60.56	62.20
OCSVM [53]	✓		65.98	83.21
LOF [6]	✓		64.63	85.25
KNN [49]	✓		64.98	84.34
AutoEncoder [26]	✓		56.34	82.13
DeepSVDD [50]	✓	✓	68.23	87.29
DeepSAD [51]	✓	✓	88.73	90.04
MultiDeepSAD* (ours)	✓	✓	91.16	92.41
MultiDeepSAD (ours)	✓	✓	93.49	95.03

Table 1: Results on SBB-AD and Open-AD datasets using different anomaly detection methods. The AUROC is reported. MultiDeepSAD* denotes the variant in which our proposed training objective in Eq. (6) is replaced with the original DeepSAD loss in Eq. (2).

Method	Force	Image	SBB-AD	Open-AD
MultiDeepSAD	✓		70.66	83.30
MultiDeepSAD		✓	89.43	91.64
MultiDeepSAD	✓	✓	93.49	95.03

Table 2: Results on SBB-AD and Open-AD datasets using different modalities.

modality-specific pseudo-anomalies in \mathcal{D}_a ensures that the model learns more robust and discriminative representations for arcing detection. Finally, we use the same Eq. (4) as in DeepSAD for inference, but propose *a new training objective* different from Eq. (2):

$$\min_{\mathbf{W}} \frac{1}{|\mathcal{D}_n|} \sum_{x_i \in \mathcal{D}_n} \|\phi(x_i; \mathbf{W}) - \mathbf{c}\|^2 + \eta \frac{1}{|\mathcal{D}_a|} \sum_{x_j \in \mathcal{D}_a} \exp(-\|\phi(x_j; \mathbf{W}) - \mathbf{c}\|^2). \quad (6)$$

Compared with the original DeepSAD anomaly term $(\|\phi(x; W) - c\|^2)^{-1}$, our exponential formulation $\exp(-\|\phi(x; W) - c\|^2)$ provides a smoother and numerically more stable optimization objective. Specifically, the original penalty is unbounded when an anomalous sample is mapped close to the center c , which can lead to gradient explosion and high sensitivity to outliers or noisy anomaly labels. In contrast, the exponential term is bounded and yields well-behaved gradients, preventing single hard samples from dominating training and improving robustness. Moreover, the exponential penalty naturally emphasizes “hard” anomalies near the decision boundary while rapidly down-weighting anomalies that have already been pushed sufficiently far from c , resulting in a more focused and stable separation between normal and anomalous representations.

5 Experiments

Implementation Details. We use ResNet-18 [25] as the encoder for images and a two-layer multilayer perceptron (MLP) for force data. The raw force signal is first transformed into the frequency domain using the Fast Fourier Transform (FFT) [45], and the first half of the normalized magnitude spectrum is retained as the input feature vector. To initialize the force encoder, we pretrain it using an autoencoder with a reconstruction loss for 100 epochs. The embeddings from the image and force encoders are then concatenated and passed through an additional two-layer MLP to obtain the final fused representation. We train all networks using the Adam optimizer [33] with a learning rate of 0.0001. The networks are trained for 30 epochs with a batch size of 64, and we set η to 1. Evaluation is performed using the Area Under Receiver Operating Characteristic curve (AUROC) as the standardized metric for all experiments.

Results on SBB-AD and Open-AD Datasets. Tab. 1 presents a comparative evaluation of various anomaly detection architectures on the SBB-AD and Open-AD datasets, using AUROC as the

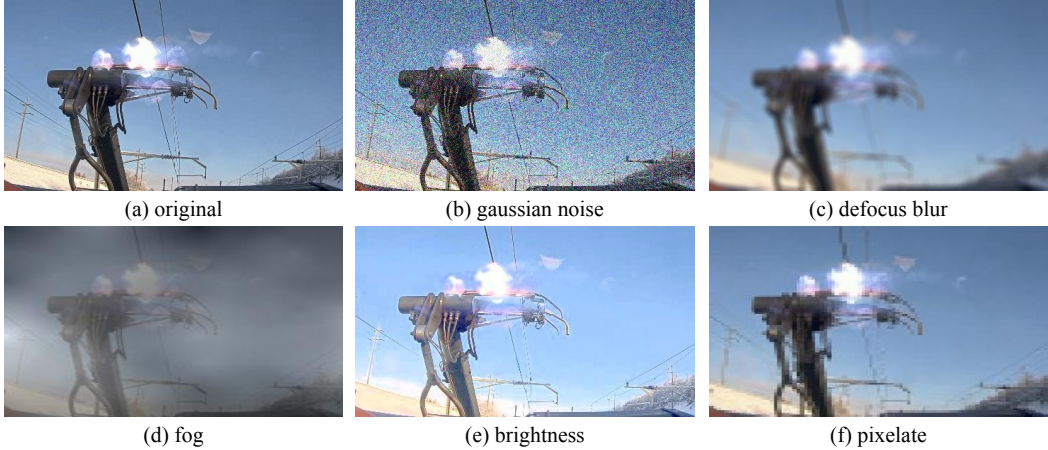


Figure 7: Illustration of different corruptions on the original image (level 3).

performance metric. The results indicate that standard unsupervised methods, including IForest [38], OCSVM [53], LOF [6], KNN [49], AutoEncoder [26], generally achieve lower performance, with AUROC scores often falling below 70% on the SBB-AD dataset. DeepSVDD [50], which incorporates both force and image data, shows a marked improvement over these classical baselines. Furthermore, DeepSAD [51] significantly outperforms the unsupervised approaches, demonstrating the substantial benefit of leveraging labeled anomalous data within a semi-supervised setting. Most notably, the proposed MultiDeepSAD method yields the highest detection accuracy on both datasets, achieving AUROC scores of 93.49% and 95.03% on SBB-AD and Open-AD, respectively, highlighting the clear advantage of our proposed training strategy and pseudo-anomaly generation method for robust arcing anomaly detection.

Tab. 2 analyzes the impact of input modalities on MultiDeepSAD performance. Using force data alone yields relatively limited accuracy (70.66% AUROC on SBB-AD and 83.30% on Open-AD), whereas using image data alone leads to a substantial improvement (89.43% and 91.64% AUROC, respectively), indicating that visual cues provide strong discriminative signals for arcing detection. Notably, combining force and image modalities achieves the best results on both datasets (93.49% on SBB-AD and 95.03% on Open-AD), demonstrating that the two modalities offer complementary information and that multimodal fusion consistently enhances robustness and overall detection performance.

Robustness to Corruptions on Images. In real-world settings, environmental conditions may vary significantly (e.g., changing from sunny to cloudy or rainy) [12], posing challenges for consistent arcing detection. Such variations often manifest as visual distortions due to lighting changes, lens contamination, or motion-induced blur in on-board monitoring systems. To simulate such distribution shifts, we evaluate our model under several common corruptions, including Gaussian noise, defocus blur, fog, brightness change, and pixelation, applied only to the image modality during testing (Fig. 7). These perturbations are selected to reflect plausible degradations in pantograph-catenary monitoring, such as reduced visibility due to weather (fog), camera defocus from vibrations, sensor noise in low-light conditions, or compression artifacts in video transmission. The model is trained on clean images using both modalities. As shown in Tab. 3, our framework maintains strong performance across most corruptions on SBB-AD. Among them, ‘fog’ has the most significant adverse impact, while other corruptions cause only minor degradation, demonstrating the model’s robustness to a wide range of visual distortions.

Robustness to the Number of Real Anomaly Samples. Tab. 4 evaluates the sensitivity of our method to the number of real anomaly samples used for pseudo-anomaly generation on the SBB-AD dataset. With only one real anomaly, the model already achieves a strong AUROC of 84.34%, demonstrating effectiveness in a highly low-shot setting. Increasing the number of real anomalies to two yields a substantial performance jump to 93.34% AUROC, after which the results remain consistently high and stable, ranging from 92.16% to 93.49% for three to five anomalies. Overall, the proposed pseudo-anomaly generation is robust to the choice of anomaly count and can reach

Corruption	AUROC (level 1)	AUROC (level 3)
Gaussian noise	91.07	89.25
Defocus blur	87.95	88.05
Fog	77.83	67.08
Brightness	92.37	87.88
Pixelate	88.89	88.28

Table 3: Results on different corruptions at different levels.

Number of real anomalies	1	2	3	4	5
AUROC	84.34	93.34	92.16	92.95	93.49

Table 4: Robustness to different numbers of real anomaly samples for pseudo-anomaly generation.

Method	Raw	Wavelet	STFT	GAF	MTF	RP	FFT
AUROC	65.66	64.22	65.27	61.00	61.86	66.24	70.66

Table 5: Ablation on different representations for force data.

Method	w/o anomaly generation	Mixup	NNG-Mix	Ours
AUROC	90.31	90.23	92.08	93.49

Table 6: Ablation on different anomaly generation methods.

near-saturated performance with only a few labeled anomalies. These results highlight the practicality of our method in scenarios where faults are extremely rare and difficult to obtain.

Ablation on Force Data Representations. The raw force signal is a one-dimensional time-series sequence that can be transformed into different representations, such as the Wavelet transform [67], short-time Fourier transform (STFT) [16], Gramian Angular Fields (GAF), Markov Transition Fields (MTF), and Recurrence Plots (RP) [60], and FFT. Overall, performance varies noticeably across feature transformations on SBB-AD: time-frequency encoding tends to be more effective than raw signals or some image-like mappings. As shown in Tab. 5, FFT achieves the best AUROC (70.66%), followed by RP (66.24%), while Raw and STFT provide comparable mid-range results (65.66% and 65.27%). Wavelet performs slightly worse (64.22%), and GAF/MTF yield the lowest AUROC (61.00% and 61.86%). These results suggest that, for force data, frequency-domain features are most informative for distinguishing arcing anomalies, whereas certain image-based time-series transforms may discard discriminative structure in this setting. Based on these findings, we use FFT as the default representation for force data in all experiments.

Comparison to Alternative Pseudo-anomaly Generation Approaches. We compare our pseudo-anomaly generation strategy with alternative approaches on SBB-AD, including Mixup [68] and NNG-Mix [11]. Mixup generates pseudo-anomalies by interpolating between anomaly and normal samples, whereas NNG-Mix uses only the nearest normal neighbors of anomaly samples for mixing. These comparison approaches were selected as representative strategies for data augmentation and semi-supervised anomaly detection, with Mixup being a widely adopted method in classification, and NNG-Mix offering a more structure-aware approach tailored to anomaly contexts. These methods were originally designed for unimodal scenarios. We extend them to multimodal settings by applying the same operations independently to each modality. As shown in Tab. 6, our method consistently outperforms both alternatives, highlighting the effectiveness of our modality-aware and targeted pseudo-anomaly generation approach when used with Multimodal DeepSAD. Interestingly, training with Mixup samples actually decreases performance. This may be due to the fact that Mixup’s image mixing strategy also blends the backgrounds, potentially diminishing the relevance of the generated anomalies for arcing detection.

Ablation on Multimodal Fusion Methods. Tab. 7 compares different multimodal fusion strategies on SBB-AD. Late fusion concatenates image and force embeddings and feeds them to an MLP to

Method	Late	Weighted	Gated	Attention
AUROC	93.49	91.56	91.61	91.84

Table 7: Ablation on multimodal fusion methods.

Model	ResNet-18	ResNet-50	ViT-B/16
AUROC	89.43	88.89	88.08

Table 8: Ablation on different image backbones.

Modality	0-shot	2-shot	4-shot	8-shot
<i>Image</i>				
RGB Images	77.37	86.89	83.07	81.28
<i>Force</i>				
Raw	46.09	49.48	48.97	48.57
RP	42.32	45.21	43.91	45.79
GAF	55.27	53.84	51.99	51.86
MTF	46.97	37.89	38.48	37.26
<i>Multimodal Fusion</i>				
RGB + GAF	74.05	73.91	83.80	76.62

Table 9: Comparison to multimodal large language models.

learn cross-modal interactions. Weighted fusion forms a convex combination of modality embeddings using learnable scalar weights. Gated fusion [1] applies learnable, per-dimension gates to modulate each modality’s contribution, optionally with modality dropout for robustness. Attention fusion [56] computes sample-wise modality weights via a softmax-based attention mechanism. Late fusion achieves the best performance with 93.49% AUROC, outperforming more complex alternatives including weighted fusion (91.56%), gated fusion (91.61%), and attention-based fusion (91.84%). This suggests that, in our setting, a straightforward late fusion of modality-specific features is sufficient to effectively exploit cross-modal complementarity, while additional learnable fusion mechanisms do not provide further gains and may introduce unnecessary optimization complexity or overfitting.

Ablation on Different Image Backbones. Tab. 8 studies the effect of different image backbones on SBB-AD. ResNet-18 achieves the best performance with 89.43% AUROC, slightly outperforming ResNet-50 (88.89%) and ViT-B/16 (88.08%) [14]. Overall, the results indicate that detection accuracy is relatively insensitive to the choice of backbone within this range, and that a lightweight CNN backbone (ResNet-18) is sufficient to provide strong visual representations for our task.

Comparison to Multimodal Large Language Models (MLLMs). MLLMs have demonstrated strong performance across a wide range of multimodal tasks involving text, images, videos, and audio. However, their effectiveness in industrial safety monitoring, such as railway arcing detection, remains underexplored. In this study, we investigate whether a general-purpose MLLM can serve as a viable alternative to traditional arcing detection methods. Specifically, we evaluate Qwen3-VL-2B-Instruct [3] and formulate arcing detection as a prompted binary classification task. The system prompt describes the visual characteristics of electrical arcing (e.g., sparks or flashes between the pantograph and the overhead contact wire) and constrains the model to output a binary decision. In the few-shot setting, we provide k annotated example images to calibrate the model to dataset-specific visual patterns. As shown in Tab. 9, the model achieves strong performance on RGB images on SBB-AD, indicating that Qwen3-VL has robust visual understanding for identifying electrical arcing. In contrast, it fails to meaningfully interpret force-based signal visualizations (Raw plots, RP, GAF, MTF), yielding near-random AUROC values, which suggests limited prior knowledge for these representations. Overall, Qwen3-VL performs substantially worse than our proposed MultiDeepSAD.

6 Conclusion

In this work, we propose a novel framework for detecting electrical arcing in pantograph-catenary systems by integrating image and force data. Our proposed MultiDeepSAD architecture extends semi-supervised anomaly detection into the multimodal domain, using pseudo-anomaly generation to make effective use of limited real anomaly data during training. Experimental results demonstrate that our multimodal approach achieves superior detection accuracy and robustness compared to baseline methods, even in the presence of domain shifts or when only a few real arcing samples are available. Ablation studies confirm the complementary value of both visual and force features for arcing detection. We also release a new multimodal dataset that includes synchronized visual and force measurements, which can serve as a challenging benchmark for future research on arcing detection in pantograph-catenary systems. From a practical standpoint, this research demonstrates that combining non-contact visual monitoring with force-based measurements enables a more reliable system for detecting arcing events. Adopting such a multimodal detection strategy has the potential to lower maintenance costs, prevent infrastructure damage, and enhance the operational reliability of rail networks. However, arcing detection alone is not sufficient to inform maintenance actions, as infrastructure risk is driven by the cumulative effect of repeated events. A practical maintenance workflow therefore requires an additional layer that consistently localizes and tracks arcing occurrences over time (i.e., linking detections to specific catenary locations and to individual pantographs) so that event frequency, duration, and severity can be aggregated into a damage or health index. Future work will explore real-time deployment on operational trains, integrate robust spatiotemporal tracking and alignment across runs, and develop lightweight cumulative damage modeling for use on resource-constrained embedded platforms.

References

- [1] John Arevalo, Thamar Solorio, Manuel Montes-y Gómez, and Fabio A González. Gated multimodal units for information fusion. *arXiv preprint arXiv:1702.01992*, 2017.
- [2] İlhan Aydin, Mehmet Karakose, and Erhan Akin. Anomaly detection using a modified kernel-based tracking in the pantograph–catenary system. *Expert Systems with Applications*, 42(2):938–948, 2015.
- [3] Shuai Bai, Yuxuan Cai, Ruizhe Chen, Keqin Chen, Xionghui Chen, Zesen Cheng, Lianghao Deng, Wei Ding, Chang Gao, Chunjiang Ge, Wenbin Ge, Zhifang Guo, Qidong Huang, Jie Huang, Fei Huang, Binyuan Hui, Shutong Jiang, Zhaohai Li, Mingsheng Li, Mei Li, Kaixin Li, Zicheng Lin, Junyang Lin, Xuejing Liu, Jiawei Liu, Chenglong Liu, Yang Liu, Dayiheng Liu, Shixuan Liu, Dunjie Lu, Ruilin Luo, Chenxu Lv, Rui Men, Lingchen Meng, Xuancheng Ren, Xingzhang Ren, Sibo Song, Yuchong Sun, Jun Tang, Jianhong Tu, Jianqiang Wan, Peng Wang, Pengfei Wang, Qiuyue Wang, Yuxuan Wang, Tianbao Xie, Yiheng Xu, Haiyang Xu, Jin Xu, Zhibo Yang, Mingkun Yang, Jianxin Yang, An Yang, Bowen Yu, Fei Zhang, Hang Zhang, Xi Zhang, Bo Zheng, Humen Zhong, Jingren Zhou, Fan Zhou, Jing Zhou, Yuanzhi Zhu, and Ke Zhu. Qwen3-vl technical report. *arXiv preprint arXiv:2511.21631*, 2025.
- [4] Sami Barmada, Marco Raugi, Mauro Tucci, and Francesco Romano. Arc detection in pantograph–catenary systems by the use of support vector machines-based classification. *IET Electrical Systems in Transportation*, 4(2):45–52, 2014.
- [5] Sami Barmada, Mauro Tucci, et al. Use of advanced signal processing techniques for arcing detection on ac pantograph catenary systems. In *IEEE International Conference on International Conference on Pantograph-Catenary Interaction Framework for Intelligent Control*, 2011.
- [6] Markus M Breunig, Hans-Peter Kriegel, Raymond T Ng, and Jörg Sander. Lof: identifying density-based local outliers. In *Proceedings of the 2000 ACM SIGMOD international conference on Management of data*, pages 93–104, 2000.
- [7] Stefano Bruni, Giuseppe Bucca, Marco Carnevale, Andrea Collina, and Alan Facchinetti. Pantograph–catenary interaction: recent achievements and future research challenges. *International Journal of Rail Transportation*, 6(2):57–82, 2018.
- [8] Richeng Chen, Yunzhi Lin, and Tao Jin. High-speed railway pantograph-catenary anomaly detection method based on depth vision neural network. *IEEE Transactions on Instrumentation and Measurement*, 71:1–10, 2022.
- [9] Liu Diyang, Gao Shibin, Luo Jiaming, Wei Xiaoguang, and Shi Jian. A reasoning approach-based pattern graph for analyzing the risk level of correlations among catenary components considering time distribution. *Reliability Engineering & System Safety*, 245:110035, 2024.

[10] Liu Diyang, Gao Shibin, Wei Xiaoguang, Luo Jiaming, and Shi Jian. Impactability and susceptibility assessment based on ds evidence theory for analyzing the risk of fault propagation among catenary components. *Reliability Engineering & System Safety*, 251:110389, 2024.

[11] Hao Dong, Gaëtan Frusque, Yue Zhao, Eleni Chatzi, and Olga Fink. Nng-mix: Improving semi-supervised anomaly detection with pseudo-anomaly generation. *IEEE Transactions on Neural Networks and Learning Systems*, 2024.

[12] Hao Dong, Moru Liu, Kaiyang Zhou, Eleni Chatzi, Juho Kannala, Cyrill Stachniss, and Olga Fink. Advances in multimodal adaptation and generalization: From traditional approaches to foundation models. *arXiv preprint arXiv:2501.18592*, 2025.

[13] Hao Dong, Yue Zhao, Eleni Chatzi, and Olga Fink. Multiod: Scaling out-of-distribution detection for multiple modalities. *Advances in Neural Information Processing Systems*, 37:129250–129278, 2024.

[14] Alexey Dosovitskiy. An image is worth 16x16 words: Transformers for image recognition at scale. *arXiv preprint arXiv:2010.11929*, 2020.

[15] Michał Dołęgowski and Mirosław Szmajda. A novel algorithm for fast dc electric arc detection. *Energies*, 14(2):288, 2021.

[16] Lutfyiye Durak and Orhan Arik. Short-time fourier transform: two fundamental properties and an optimal implementation. *IEEE Transactions on Signal Processing*, 51(5):1231–1242, 2003.

[17] M Elia, Giorgio Diana, M Bocciolone, Stefano Bruni, Federico Cheli, Andrea Collina, and Ferruccio Resta. Condition monitoring of the railway line and overhead equipment through onboard train measurement—an italian experience. In *IET International Conference on Railway Condition Monitoring*, 2006.

[18] Olga Fink, Ismail Nejjar, Vinay Sharma, Keivan Faghah Niresi, Han Sun, Hao Dong, Chenghao Xu, Amaury Wei, Arthur Bizzi, Raffael Theiler, et al. From physics to machine learning and back: Part ii-learning and observational bias in phm. *arXiv preprint arXiv:2509.21207*, 2025.

[19] Olga Fink, Vinay Sharma, Ismail Nejjar, Leandro Von Krannichfeldt, Sergei Garmaev, Zepeng Zhang, Amaury Wei, Gaetan Frusque, Florent Forest, Mengjie Zhao, et al. From physics to machine learning and back: Part i-learning with inductive biases in prognostics and health management. *Reliability Engineering & System Safety*, page 112213, 2026.

[20] Guoqiang Gao, Xin Yan, Zefeng Yang, Wenfu Wei, Yi Hu, and Guangning Wu. Pantograph–catenary arcing detection based on electromagnetic radiation. *IEEE Transactions on Electromagnetic Compatibility*, 61(4):983–989, 2018.

[21] SB Gao, ZG Liu, and Long Yu. Detection and monitoring system of the pantograph–catenary in high-speed railway (6c). In *2017 7th International conference on power electronics systems and applications-smart mobility, power transfer & security (PESA)*, pages 1–7, 2017.

[22] Shibin Gao. Automatic detection and monitoring system of pantograph–catenary in china’s high-speed railways. *IEEE Transactions on Instrumentation and Measurement*, 70:1–12, 2020.

[23] Izhak Golan and Ran El-Yaniv. Deep anomaly detection using geometric transformations. *Advances in neural information processing systems*, 31, 2018.

[24] S Gregori, M Tur, J Gil, and FJ Fuenmayor. Assessment of catenary condition monitoring by means of pantograph head acceleration and artificial neural networks. *Mechanical Systems and Signal Processing*, 202:110697, 2023.

[25] Kaiming He, Xiangyu Zhang, Shaoqing Ren, and Jian Sun. Deep residual learning for image recognition. In *Proceedings of the IEEE conference on computer vision and pattern recognition*, pages 770–778, 2016.

[26] Geoffrey E Hinton and Ruslan R Salakhutdinov. Reducing the dimensionality of data with neural networks. *science*, 313(5786):504–507, 2006.

[27] Jonathan Ho, Ajay Jain, and Pieter Abbeel. Denoising diffusion probabilistic models. *Advances in neural information processing systems*, 33:6840–6851, 2020.

[28] Chen Hong-ming, Zhou Ning, Cheng Yao, and Zhang Wei-hua. Non-contact detection method for pantograph–catenary contact force based on image processing. *Proceedings of the Institution of Mechanical Engineers, Part F: Journal of Rail and Rapid Transit*, 238(7):745–756, 2024.

[29] Shize Huang, Wei Chen, Bo Sun, Ting Tao, and Lingyu Yang. Arc detection and recognition in the pantograph–catenary system based on multi-information fusion. *Transportation Research Record*, 2674(10):229–240, 2020.

[30] Shize Huang, Liangliang Yu, Fan Zhang, Wei Zhu, and Qiyi Guo. Cluster analysis based arc detection in pantograph–catenary system. *Journal of Advanced Transportation*, 2018(1):1329265, 2018.

[31] Shize Huang, Yachan Zhai, Miaomiao Zhang, and Xiaoxue Hou. Arc detection and recognition in pantograph–catenary system based on convolutional neural network. *Information Sciences*, 501:363–376, 2019.

[32] Gulsah Karaduman, Mehmet Karakose, and Erhan Akin. Deep learning based arc detection in pantograph-catenary systems. In *2017 10th International Conference on Electrical and Electronics Engineering (ELECO)*, pages 904–908, 2017.

[33] Diederik P Kingma. Adam: A method for stochastic optimization. *arXiv preprint arXiv:1412.6980*, 2014.

[34] Demetris Lappas, Vasileios Argyriou, and Dimitrios Makris. Dynamic distinction learning: adaptive pseudo anomalies for video anomaly detection. In *Proceedings of the IEEE/CVF Conference on Computer Vision and Pattern Recognition*, pages 3961–3970, 2024.

[35] Bin Li, Jiahui Shu, and Diansong Du. Theoretical modeling and fault diagnosis of pantograph–catenary arc under high-speed airflow. *Scientific Reports*, 15(1):9233, 2025.

[36] Chun-Liang Li, Kihyuk Sohn, Jinsung Yoon, and Tomas Pfister. Cutpaste: Self-supervised learning for anomaly detection and localization. In *Proceedings of the IEEE/CVF conference on computer vision and pattern recognition*, pages 9664–9674, 2021.

[37] Haoqian Li, Yong Wang, Jing Zeng, Fansong Li, Zhenhuan Yang, Guiming Mei, and Yunguang Ye. Virtual point tracking method for online detection of relative wheel-rail displacement of railway vehicles. *Reliability Engineering & System Safety*, 246:110087, 2024.

[38] Fei Tony Liu, Kai Ming Ting, and Zhi-Hua Zhou. Isolation forest. In *2008 eighth ieee international conference on data mining*, pages 413–422, 2008.

[39] Moru Liu, Hao Dong, Jessica Kelly, Olga Fink, and Mario Trapp. Extremely simple multimodal outlier synthesis for out-of-distribution detection and segmentation. *arXiv preprint arXiv:2505.16985*, 2025.

[40] Xiaohong Liu, Xiaoyu Wang, Wei Quan, Guoxin Gu, Xiaoqian Xu, and Shabin Gao. A pantograph-catenary arcing detection model for high-speed railway based on semantic segmentation and generative adversarial network. *International Journal of Rail Transportation*, pages 1–22, 2024.

[41] Yang Liu, Wei Quan, Xuemin Lu, Xiaohong Liu, Shabin Gao, Haiquan Zhao, Long Yu, and Jie Zheng. A novel arcing detection model of pantograph–catenary for high-speed train in complex scenes. *IEEE Transactions on Instrumentation and Measurement*, 72:1–13, 2023.

[42] Andrea Mariscotti. The electrical behaviour of railway pantograph arcs. *Energies*, 16(3):1465, 2023.

[43] Yutao Mo, Yizhen Peng, Jing Wu, and Kangbo Fan. Knowledge-embedding deep interpretable graph model for wear prediction: Application in pantograph-catenary systems. *Reliability Engineering & System Safety*, 261:111140, 2025.

[44] Ismail Nejjar, Hao Dong, and Olga Fink. Recall and refine: A simple but effective source-free open-set domain adaptation framework. *arXiv preprint arXiv:2411.12558*, 2024.

[45] Henri J Nussbaumer and Henri J Nussbaumer. *The fast Fourier transform*. Springer, 1982.

[46] Carmine M Pappalardo, Mohil D Patel, Brian Tinsley, and Ahmed A Shabana. Contact force control in multibody pantograph/catenary systems. *Proceedings of the Institution of Mechanical Engineers, Part K: Journal of Multi-body Dynamics*, 230(4):307–328, 2016.

[47] Wei Quan, Shaopeng Guo, Xuemin Lu, Guoxin Gu, Wenjing Cheng, Ning Zhou, and Long Yu. Arcmask: a robust and fast image-based method for high-speed railway pantograph-catenary arcing instance segmentation. *Neural Computing and Applications*, 35(9):6875–6890, 2023.

[48] Wei Quan, Xiaoqian Xu, Xiaolin Liu, Xiaoyu Wang, and Shabin Gao. Arcse: A dual-branch semantic segmentation model for robust pantograph-catenary arcing detection in complex environments. *IEEE Transactions on Instrumentation and Measurement*, 2024.

[49] Sridhar Ramaswamy, Rajeev Rastogi, and Kyuseok Shim. Efficient algorithms for mining outliers from large data sets. In *Proceedings of the 2000 ACM SIGMOD international conference on Management of data*, pages 427–438, 2000.

[50] Lukas Ruff, Robert Vandermeulen, Nico Goernitz, Lucas Deecke, Shoaib Ahmed Siddiqui, Alexander Binder, Emmanuel Müller, and Marius Kloft. Deep one-class classification. In *International conference on machine learning*, pages 4393–4402. PMLR, 2018.

[51] Lukas Ruff, Robert A Vandermeulen, Nico Görnitz, Alexander Binder, Emmanuel Müller, Klaus-Robert Müller, and Marius Kloft. Deep semi-supervised anomaly detection. *arXiv preprint arXiv:1906.02694*, 2019.

[52] Thomas Schlegl, Philipp Seeböck, Sebastian M Waldstein, Georg Langs, and Ursula Schmidt-Erfurth. f-anogan: Fast unsupervised anomaly detection with generative adversarial networks. *Medical image analysis*, 54:30–44, 2019.

[53] Bernhard Schölkopf, John C Platt, John Shawe-Taylor, Alex J Smola, and Robert C Williamson. Estimating the support of a high-dimensional distribution. *Neural computation*, 13(7):1443–1471, 2001.

[54] Han Sun, Yunkang Cao, Hao Dong, and Olga Fink. Unseen visual anomaly generation. In *Proceedings of the Computer Vision and Pattern Recognition Conference*, pages 25508–25517, 2025.

[55] Mengying Tan, Haishangyang Li, and Lei Nie. Defect diagnosis of rigid catenary system based on pantograph vibration performance. In *Actuators*, volume 13, page 162. MDPI, 2024.

[56] Ashish Vaswani, Noam Shazeer, Niki Parmar, Jakob Uszkoreit, Llion Jones, Aidan N Gomez, Łukasz Kaiser, and Illia Polosukhin. Attention is all you need. *Advances in neural information processing systems*, 30, 2017.

[57] Jian Wang, Shabin Gao, Long Yu, Xingyang Liu, Ferrante Neri, Dongkai Zhang, and Lei Kou. Uncertainty-aware trustworthy weather-driven failure risk predictor for overhead contact lines. *Reliability Engineering & System Safety*, 242:109734, 2024.

[58] Jian Wang, Shabin Gao, Long Yu, Chaoqun Ma, Dongkai Zhang, and Lei Kou. A data-driven integrated framework for predictive probabilistic risk analytics of overhead contact lines based on dynamic bayesian network. *Reliability Engineering & System Safety*, 235:109266, 2023.

[59] Ying Wang, Zhigang Liu, Fuqiang Fan, and S Bin Gao. Review of research development of pantograph-catenary arc model and electrical characteristics. *Journal of the China Railway Society*, 35(8):35–43, 2013.

[60] Zhiguang Wang, Tim Oates, et al. Encoding time series as images for visual inspection and classification using tiled convolutional neural networks. In *AAAI Workshops*, 2015.

[61] Guangning Wu, Guoqiang Gao, Wenfu Wei, Zefeng Yang, Guangning Wu, Guoqiang Gao, Wenfu Wei, and Zefeng Yang. Diagnosis and detection of service performance of pantograph and catenary. *The Electrical Contact of the Pantograph-Catenary System: Theory and Application*, pages 221–278, 2019.

[62] Wu Xinyuan, Gao Shabin, Wei Xiaoguang, Liu Diyang, and Ling Weize. Causal correlation inference between fault catenary components based on kolmogorov complexity. *Reliability Engineering & System Safety*, page 111805, 2025.

[63] Jingke Yan, Yao Cheng, Fan Zhang, Mudi Li, Ning Zhou, Bo Jin, Hui Wang, Haonan Yang, and Weihua Zhang. Research on multimodal techniques for arc detection in railway systems with limited data. *Structural Health Monitoring*, page 14759217251336797, 2025.

[64] Yue Yan, Hu Liu, Linfeng Gan, and Runtong Zhu. A novel arc detection and identification method in pantograph-catenary system based on deep learning. *Scientific Reports*, 15(1):3511, 2025.

[65] Gang Yang, Guowei Kong, and Xin Shen. Arc recognition for pantograph-catenary system of railway using current. *Measurement*, 251:117304, 2025.

[66] Qiongfang Yu, Yaqian Hu, and Yi Yang. Identification method for series arc faults based on wavelet transform and deep neural network. *Energies*, 13(1):142, 2019.

[67] Dengsheng Zhang. Wavelet transform. In *Fundamentals of image data mining: Analysis, Features, Classification and Retrieval*, pages 35–44. Springer, 2019.

[68] Hongyi Zhang, Moustapha Cisse, Yann N Dauphin, and David Lopez-Paz. mixup: Beyond empirical risk minimization. In *International Conference on Learning Representations*, 2018.